A histopathological classification system of Tyr::NRAS^{Q61K} murine melanocytic lesions: A reproducible simplified classification

Pierre Sohier | Léa Legrand | Zackie Aktary |
Christine Grill | Véronique Delmas | Florence Bernex |
Edouard Reyes-Gomez |Lionel Larue | Béatrice Vergier

If you wish to order reprints of this article,
please see the guidelines **here**

Supporting Information for this article is freely available **here**

EMAIL ALERTS
Receive free email alerts and stay up-to-date on what is published
in Pigment Cell & Melanoma Research – **click here**

Submit your next paper to PCMR online at http://mc.manuscriptcentral.com/pcmr

Subscribe to PCMR and stay up-to-date with the only journal committed to publishing
basic research in melanoma and pigment cell biology

As a member of the IFPCS or the SMR you automatically get online access to PCMR. Sign up as
a member today at **www.ifpcs.org** or at **www.societymelanomaresarch.org**

To take out a personal subscription, please click here
More information about Pigment Cell & Melanoma Research at **www.pigment.org**

ORIGINAL ARTICLE

WILEY

A histopathological classification system of Tyr::NRAS^{Q61K} murine melanocytic lesions: A reproducible simplified classification

Pierre Sohier[1,2,3†] | Léa Legrand[4,5†] | Zackie Aktary[1,2,3] | Christine Grill[1,2,3] | Véronique Delmas[1,2,3] | Florence Bernex[6] | Edouard Reyes-Gomez[7,8,9] | Lionel Larue[1,2,3‡] (iD) | Béatrice Vergier[4,5‡]

[1]Institut Curie, INSERM U1021, Normal and Pathological Development of Melanocytes, PSL Research University, Orsay, France

[2]CNRS UMR3347, Univ Paris-Sud, Univ Paris-Saclay, Orsay, France

[3]Equipe Labellisée Ligue Contre le Cancer, Orsay, France

[4]INSERM U1053, Team 3 Oncogenesis of Cutaneous Lymphomas, Univ. Bordeaux, Bordeaux, France

[5]Pathology Department, CHU Bordeaux, Pessac, France

[6]IRCM, Inserm, ICM, Univ Montpellier, Montpellier, France

[7]INRA, UMR955 Génétique Fonctionnelle et Médicale, Ecole Nationale Vétérinaire d'Alfort, Maisons-Alfort, France

[8]UMR955 Génétique Fonctionnelle et Médicale, Ecole Nationale Vétérinaire d'Alfort, Université Paris-Est, Maisons-Alfort, France

[9]Unité d'Embryologie, d'Histologie et d'Anatomie Pathologique, Ecole Nationale Vétérinaire d'Alfort, Université Paris-Est, Maisons-Alfort, France

Correspondence
L. Larue
Email: lionel.larue@curie.fr

Summary

Genetically engineered mouse models offer essential opportunities to investigate the mechanisms of initiation and progression in melanoma. Here, we report a new simplified histopathology classification of mouse melanocytic lesions in Tyr::NRAS^{Q61K} derived models, using an interactive decision tree that produces homogeneous categories. Reproducibility for this classification system was evaluated on a panel of representative cases of murine melanocytic lesions by pathologists and basic scientists. Reproducibility, measured as inter-rater agreement between evaluators using a modified Fleiss' *kappa* statistic, revealed a very good agreement between observers. Should this new simplified classification be adopted, it would create a robust system of communication between researchers in the field of mouse melanoma models.

KEYWORDS

β-catenin, histopathology, Ink4a, melanocyte, melanoma, melanoma model, Pten, Ras, transgenic mice

---

†These authors contributed equally to this work.

‡Co-last-authors.

1 | INTRODUCTION

Genetically engineered mouse (GEM) models have proven successful in modeling human melanoma (Conde-Perez & Larue, 2014; Frese & Tuveson, 2007). Mice provide a relevant tool to study specific hypotheses through genetic engineering to recapitulate the molecular events of melanoma initiation and metastatic progression. A wide variety of mouse models have been generated over the years using techniques such as random integration, homologous recombination, and most recently, Cre/CreER[T2]-LoxP recombination (Larue & Beermann, 2007). The most recent techniques allow for spatial and temporal control of transgenes. One widely used mouse melanoma model in the literature is the Tyr::NRAS[Q61K] model, which exhibits melanocyte-specific expression of the mutated human *NRAS* gene encoding Q61K oncoprotein under the control of the tyrosinase distal regulatory element (DRE) and the promoter of the mouse tyrosinase gene (Ackermann et al., 2005). These mice develop cutaneous melanoma with metastatic dissemination, primarily to the lymph nodes and then to the lung and liver. Thus, this mouse model recapitulates some of the sequential steps of melanoma formation and progression. The Tyr::NRAS[Q61K] (NRAS) model has been used in combination with oncogenes or tumor suppressors. The Tyr::NRAS[Q61K]; Ink4a-Arf^{+/−} (NRAS;Ink4a) or Tyr::NRAS[Q61K]; and Ink4a-Arf^{−/−} (NRAS;Ink4a-) models, which carry a mono- or bi-allelic deletion of the INK4a/Cdkn2a locus (encoding p16[INK4a] and p19[ARF]), show a shorter latency and increased frequency of melanoma formation than NRAS mice (Ackermann et al., 2005). The Tyr::NRAS[Q61K]; Tyr::bcat[sta] (NRAS;bcat*) model expresses a stabilized and activated form of β-catenin under the control of the tyrosinase DRE and promoter (Delmas et al., 2007). These mice develop melanoma with a latency and frequency similar to that of Ink4a-Arf-deficient mice. The Tyr::Nras[Q61K]; Tyr::Cre; Pten[F/+] (NRAS;Pten) model develops cutaneous melanomas with a higher penetrance and a shorter latency than NRAS mice (Conde-Perez et al., 2015). Microscopically, melanocytic lesions in these mouse melanoma models demonstrate a morphological spectrum ranging from early precursor lesions, showing similarities to nevi, to larger tumors, showing similarities to human cutaneous melanoma. A classification for mouse melanocytic lesions stemming from the NRAS mouse melanoma model has been proposed by human and veterinary pathologists (Campagne et al., 2013). However, the current shortage of human and veterinary pathologists with mouse expertise has compelled researchers to rely on their own "*Do-it-Yourself*" pathology (Barthold et al., 2007; Cardiff, 2007). Although there are legitimate concerns with this approach, namely an inconsistency in the way samples are scored and classified, the trend is unavoidable and will continue in the near future (Cardiff, Ward, & Barthold, 2008). Given this context, there is a strong need for a robust and reproducible classification system that produces homogeneous categories for melanocytic lesions.

Here, we propose a new simplified framework for routine classification of mouse melanocytic lesions, using an interactive decision tree. We believe that following the classification framework proposed here may help to avoid major errors in classification. The goal of this

Significance

Genetically engineered melanoma mouse models are a mainstay of modern melanoma research and are essential for investigating tumor initiation and progression as well as a promising method to screen melanoma therapies. Here, we report a simplified and user-friendly histopathology classification of mouse melanoma model.

classification is to allow researchers to define reproducible homogenous subgroups of melanocytic lesions in mouse models for further studies. We successfully demonstrate reproducibility between pathologist and non-pathologist researchers using this simplified classification.

2 | RESULTS

2.1 | Basis of the classification methodology

A decision tree-based classification was built using nine criteria and refined to achieve an optimal balance between efficiency, simplicity, and reproducibility. Criteria were evaluated on a panel of 46 independent mouse melanocytic lesions from five different genotypes: NRAS, NRAS;Ink4a, NRAS;bcat*, NRAS;Pten, and NRAS;Ink4a;bcat*. We defined five categories of melanocytic lesions according to distinctive morphological features and expected biological behavior. Two categories (MLP1 and MLP2) encompass Melanocytic Lesion Precursor (MLP), demonstrating dermal proliferation of melanocytes following the expression of the NRAS[Q61K] oncogene in all melanocytes. These lesions are invariably present to varying degrees in all NRAS mice after a few months of life. MLP2 differs from MLP1 by the presence of clusters of melanocytes. Three categories encompass melanocytic tumors (MT1, MT2, and MT3) demonstrating distinct morphological features, each supporting an increasingly malignant potential. These categories differ from those described in the previous classification (Campagne et al., 2013). Certain melanocytic lesions are associated with multiple categories, often combining a precursor lesion (MLP1 or MLP2) with another category (MT1, MT2, or MT3). In this case, the highest grade type of lesion takes precedence over the lowest. Retained criteria for the classification were (i) location of the tumor in the skin layers, (ii) shape of the proliferation, (iii) presence of clusters of melanocytes in the dermis, (iv) presence of necrosis, (v) presence of significant cytological atypia, (vi) presence of mitosis, (vii) epidermal ulceration, (viii) tumor circumscription, (ix) and presence of distinctive vascularization patterns.

1. The determination of the location of the lesion is the first step in the decision tree. MLP1 and MLP2 lesions are limited to the dermis, whereas MT1, MT2, and MT3 lesions are dermal lesions that also extend to subcutaneous fat (Figure S1a,b).

2. The second discriminating feature is the shape of the proliferation. MLP1 and MLP2 lesions most often demonstrate diffuse, discontinuous, multifocal proliferations of melanocytes that wrap around the hair follicles, without disruption of the skin architecture (Figure 1a-c). This pattern generally appears as a horizontal pigmented dermal band, which has been described previously (Wurm et al., 2012). MT1, MT2, and MT3 lesions show a more typical tumoral aspect, often with a rounded bulging lesion that pushes back the preexisting anatomical structures (Figure S1c,d).

3. The presence of clusters of densely packed melanocytes allows discrimination between MLP1 and MLP2 lesions. These melanocytes tend to be larger and have a rounder, more visible nucleus (Figure 1d).

   Melanocytic lesions extending beyond the dermis and showing a tumoral aspect may present three major criteria (4 to 6).

4. The presence of necrosis is considered to favor malignancy. Necrosis consists of cell death with the loss of membrane integrity and enzymatic destruction of the cellular constituents. The observed microscopic changes reflect these processes (Herrington, 2014). Necrotic cells stain pink with routine H&E staining and lack definition under the microscope, taking on a ghostly appearance. Nuclear changes include the loss of staining (karyolysis), shrinkage (pyknosis), and fragmentation (karyorrhexis). Eventually, the nucleus disappears completely. This appearance can be modified by the presence of inflammatory cells, including neutrophils and macrophages. Practical recognition of necrosis should focus on spotting areas of pink eosinophilic material at intermediate magnification. In some cases, necrosis may be stained with melanin in heavily pigmented tumors, giving a deceptive "brownish" appearance (Figure 2a,b).

5. The presence of significant cytological atypia is also considered to favor malignancy. In general, the degree of atypia correlates with the aggressiveness of the tumor. Cytological evidence of atypia includes variation in the size and shape of cells (pleomorphism), enlarged and hyperchromatic nuclei with coarsely clumped chromatin and prominent nucleoli, and bizarre cells. Only cytological atypia deemed "severe" was considered to be significant for classification purpose (Figure 2e,f, Figure S2a,b).

6. The presence of mitoses is considered to favor malignancy. Abundant mitoses are characteristic of many melanomas. Pathologists usually count mitotic figures and express them as
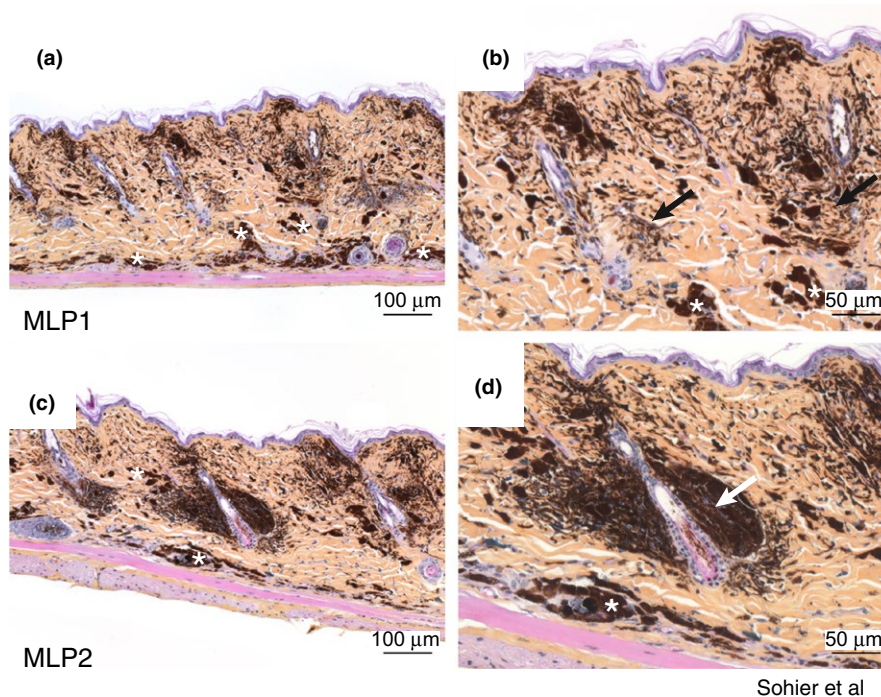

FIGURE 1 Criteria for classification of melanocytic lesions in Tyr::Nras^{Q61K} mouse model. Shape of melanocytic lesion precursor (MLP)1 and MLP2 lesions and presence of clusters of melanocytes in the dermis. (a) Histopathological appearance of an MLP1 case. MLP1 and MLP2 lesions demonstrate diffuse discontinuous multifocal proliferation of melanocytes that wrap around the hair follicles, without disruption of the skin architecture. Aggregates of pigmented macrophages containing melanin are visible (white asterisks) and should not be mistaken for tumor extension. (b) Higher magnification of A. Detail of melanocyte proliferation showing pigmented spindle-shaped cells (black arrows). A few melanophages are present (white asterisks). (c) Histopathological appearance of an MLP2 case. MLP2 lesions demonstrate additional features compared to MLP1 with rounded dense clusters of cells. (d) Higher magnification of (c). Clusters of melanocytes (white arrow) showing larger, rounder cells intermingled with melanophages (white asterisk). HES (hematoxylin eosin saffron) staining. Bars: (a,c) = 200 μm; (b,d) = 50 μm [Colour figure can be viewed at wileyonlinelibrary.com]
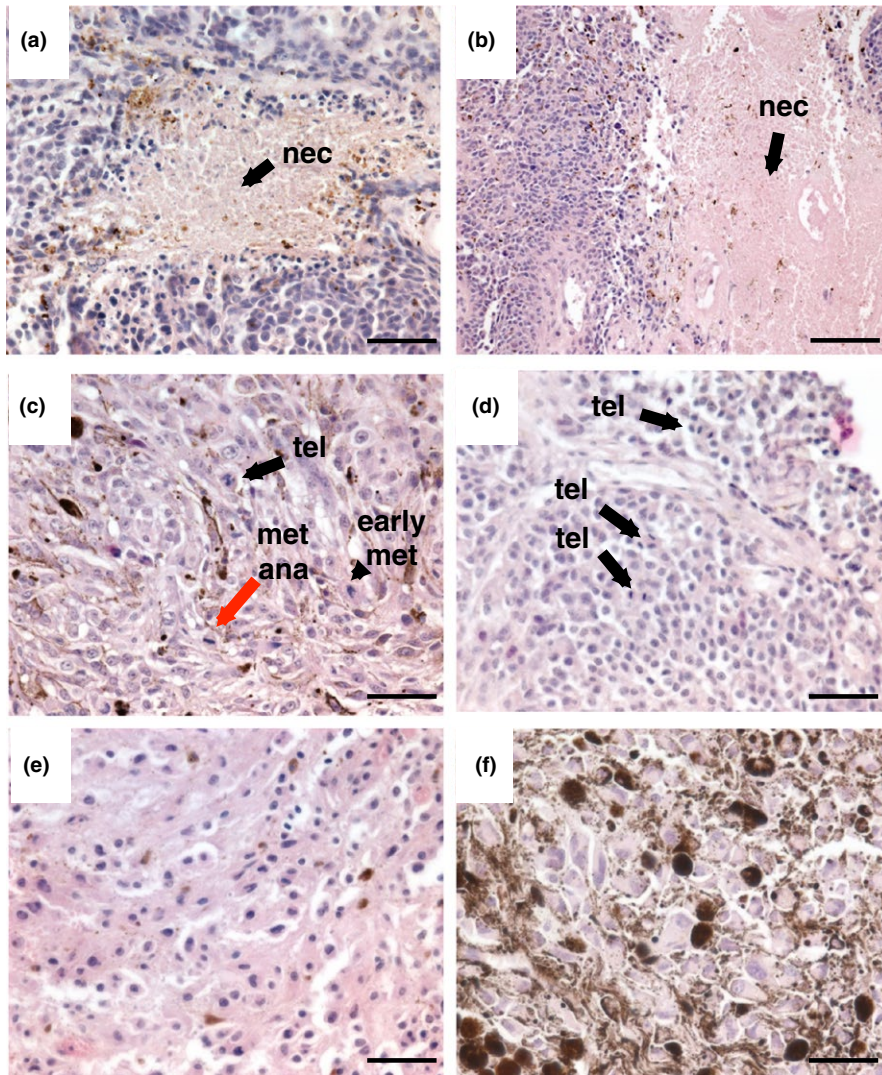
FIGURE 2 Major criteria for malignancy in melanocytic lesions in Tyr::Nras^{Q61K} mouse model. (a, b) Histopathological appearance of tumoral necrosis, demonstrating areas of pink eosinophilic necrotic (Nec) material (black arrows). There is a small amount of melanin staining of the necrosis for both cases. (c, d) Tumors demonstrating different aspects of mitotic figures (arrows and arrowheads). Condensed chromosomes are visible as clumped (beginning metaphase [early met], (c): arrowhead), in a plane (metaphase–anaphase [met-ana], (c): red arrow), or in separate chromosomal aggregates (telophase [tel], (d): arrows). (e) Tumor demonstrating mild non-significant levels of atypia, including moderate variations in the size and shape of the cells and small nuclei with dense chromatin and no visible nucleoli. (f) Tumor demonstrating very high levels of atypia, including large variations in the size and shape of the cells (pleomorphism) and enlarged and hyperchromatic nuclei with coarsely clumped chromatin and prominent nucleoli. H&E stains at a magnification of 200 (b) and 400 (a, c–f). Bars: (a, c–f) = 50 μm; (b) = 100 μm [Colour figure can be viewed at wileyonlinelibrary.com]

the number of mitotic figures per high-power (×400) field or the number of mitoses per square millimeter. We deliberately chose to simplify the classification system and used a binary system. Mitoses are either "easy to find" when they are readily identified, after screening a few fields at high power (×400), or absent if no mitotic figures are found after screening a few fields. Precise criteria for recognizing mitotic figures should be applied to achieve interobserver concordance (Van Diest et al., 1992; Weidner, Cote, Suster, & Weiss, 2009). The nuclear membrane must be absent to qualify as a mitotic figure, indicating that the cells have gone through prophase. Clear, hairy extensions of nuclear material (condensed chromosomes) must be present. They can be clumped (beginning metaphase), in a plane (metaphase–anaphase), or in separate chromosomal aggregates (telophase). Features suggesting that a "mitotic object" is not a true mitosis include small, regular extensions (not hairy) with a central empty zone, separate dark, round nuclear clumps or apoptotic nuclear segments, and orange shrunken-appearing cytoplasm. If there is doubt, the object should not be counted as a true mitosis.

If melanocytic lesions have none of these three criteria (necrosis, mitosis, or cytological atypia), they are classified as MT1 melanocytic tumors, encompassing all melanocytic tumors of low malignant potential. When cases have two or three of these major criteria, they are directly classified in category MT3, encompassing melanocytic tumors with overtly malignant features.

When only one criterion is present, appreciation of the further criteria is required to distinguish MT2 from MT3 lesions. Three minor criteria are used to refine the classification (7 to 9).

7. Epidermal ulceration is defined by a full-thickness defect of the epidermis, with evidence of host response (i.e., fibrin deposition, presence of neutrophils, reactive changes of the surrounding epidermis).

The presence of neutrophils or associated epidermal reactive changes of adjacent epidermis are required to differentiate true ulceration from postmortem removal of the epidermis. A detailed illustration with annotations is available in Figure 3a,b.

8. Tumor circumscription is an informative clue to evaluate the aggressive nature of melanocytic lesions. Smooth contours with sharp lateral circumscription favor a slowly evolving lesion. Lesions with irregular, infiltrating margins are considered to be more aggressive. This criterion is best appreciated at low magnification (Figure 4 a,b). Melanin-containing macrophages, called melanophages, are often present within the tumor or scattered in the surrounding dermis and subcutaneous fat. In some cases, differentiating melanophages outside the tumor from authentic tumor extensions can be tricky.

9. The presence of two possible specific vascularization patterns is a model-specific criterion. A pattern of pseudopapillary vascularization, previously described as "pseudo-rosette," is more frequently observed in melanocytic lesions when other morphological features evocative of malignancy are present (Campagne et al., 2013). Characteristic pseudopapillary architecture demonstrates numerous blood vessels surrounded by tumor cells, in which cells distant from the blood vessels tend to lose cohesiveness and degenerate. This gives the appearance of a cuff of viable tumor cells surrounding each blood vessel (Figure 5a).

The presence of hemangiopericytic-type vascularization is a novel, previously undescribed criterion for malignancy in murine melanocytic lesions. It is similarly associated with other morphological features indicative of malignancy. In this pattern, blood vessels form a continuous, ramifying network that exhibits striking variation in caliber. Typically, dilated branching vessels divide in a staghorn or antler-like configuration (Figure 5b).

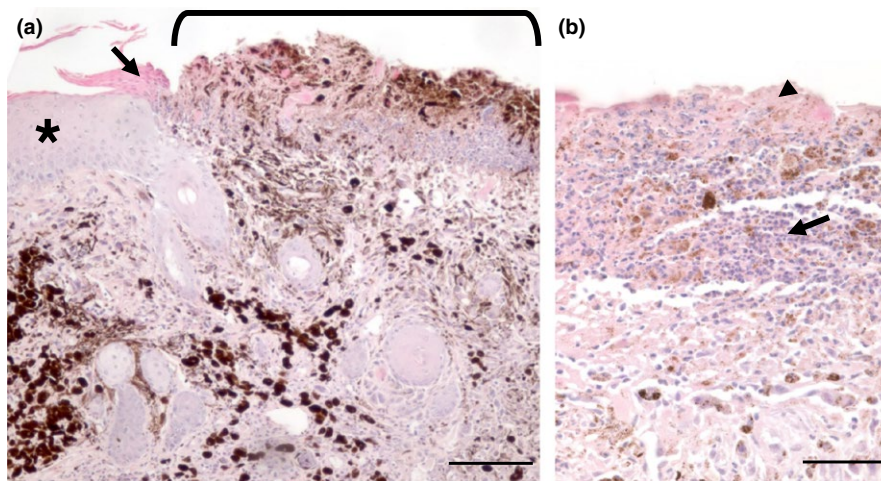All nine criteria are gathered in a decision tree (Figure 6).

FIGURE 3 Ulceration is a minor criterion for malignancy in melanocytic lesions in NRAS mouse models. (a) Histopathological appearance of ulceration. Full-thickness defect of the epidermis replaced by fibrin and cell debris containing neutrophils (horizontal bracket). There is melanin staining of the fibrin in the upper layer. Note the adjacent intact epidermis (black asterisk) with associated reactive changes, including parakeratosis (black arrow). Parakeratosis is a type of keratinization characterized by nuclei that are retained in the stratum corneum. The multiplicity of possible reactive changes is beyond the scope of this article. (b) Histopathological appearance, showing detail of ulceration with the presence of fibrin (pink material, arrowhead) and neutrophils (black arrow). Some extracellular melanin is present. H&E stains at a magnification of 100 (a) and 400 (b). Bars: (a) = 200 μm; (b) = 50 μm [Colour figure can be viewed at wileyonlinelibrary.com]
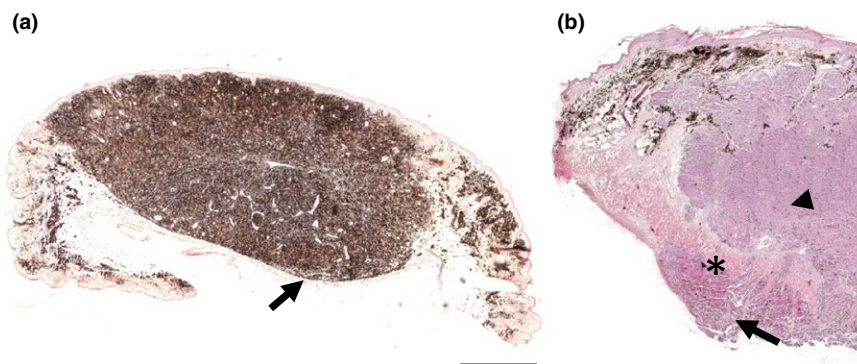

FIGURE 4 Tumor circumscription is a minor criterion for malignancy in melanocytic lesions in NRAS mouse models. (a) Histopathological appearance of a well-delineated tumor, demonstrating smooth contours with sharp lateral circumscription (arrow). (b) Histopathological appearance of a poorly limited tumor. The tumor (arrowhead) presents an extension (arrow) seen passing into and beyond the striated muscle (black asterisk) with irregular edges infiltrating down to the specimen resection margin. H&E stains at a magnification of ×20 for (a), and ×25 for (b). Bars: (a) = 1 mm; (b) = 0.8 mm [Colour figure can be viewed at wileyonlinelibrary.com]
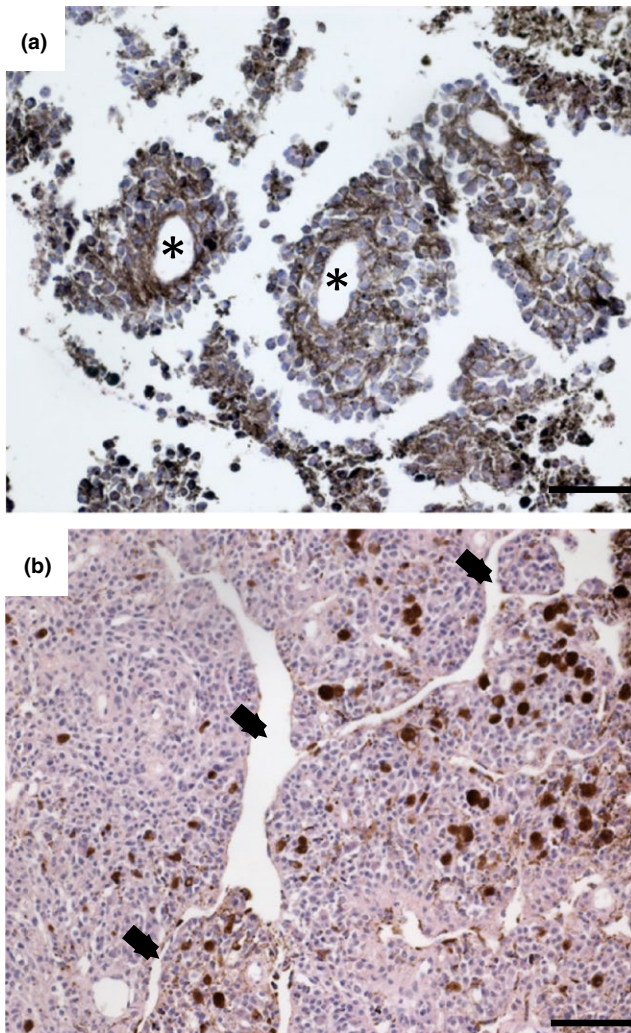
FIGURE 5 The presence of specific vascularization patterns is a minor criterion for malignancy in melanocytic lesions in NRAS mouse melanoma models. (a) Histopathological appearance of pseudopapillary-type pattern. Pseudopapillary architecture demonstrates numerous blood vessels (black asterisk) surrounded by tumor cells, in which cells distant from the blood vessels tend to lose cohesiveness and degenerate, giving the appearance of a cuff of viable tumor cells around each blood vessel. (b) Histopathological appearance of a hemangiopericytic-type pattern. Blood vessels (arrows) form a continuous, ramifying network that exhibits striking variation in caliber. These dilated branching vessels divide in a staghorn configuration. H&E stains at a magnification of 200 (a-b). Bars: (a, b) = 100 μm [Colour figure can be viewed at wileyonlinelibrary.com]

2.2 | Validation of the classification

Reproducibility for this classification system was evaluated on a panel of 20 representative cases of murine melanocytic lesions chosen from among the 46 cases available. Raters consisted of one human pathologist and two biology researchers with no previous experience in the histopathological assessment of melanoma. Raters were free to familiarize themselves with the classification on the whole dataset prior to evaluation. Inquiries about specific criteria were answered. No further training was provided. Raters were asked to evaluate items pertaining to the classification and determine the class label for each case. They were provided with a step-by-step interactive version of the classification (Figure S4). Reproducibility was measured as inter-rater agreement between evaluators using a modified Fleiss' *kappa* statistic (s*) generalized to the case of ordinal variables using linear weights (Marasini, Quatto, & Ripamonti, 2016). Computation of the s* statistic was performed using the R environment for statistical computing and the *raters* package (Quatto & Ripamonti, 2014; R-Core-Team, 2017). Statistics for pairwise interobserver agreement using a weighted Cohen's *kappa* statistic were also computed. Characteristics for the 20 cases of the evaluation panel are listed in Table S1. The pathologist found the following repartition of cases among the different categories: 10% MLP2 (2/20), 30% MT1 (6/20), 20% MT2 (4/20), and 40% MT3 (8/20). No case was diagnosed as MLP1. We compared this distribution with that obtained by the two other raters (Figure 7a).

Inter-rater agreement, expressed as the s* statistic, was 0.76. According to Fleiss' qualitative scale, values of *kappa* greater than 0.75 are considered to be evidence of "very good" agreement between observers (Fleiss, Levin, & Paik, 2003). Respective paired agreements between each biology researcher and the pathologist, measured using a weighted Cohen's *kappa* statistic, were 0.78 and 0.74. We determined whether discrepancies were randomly distributed among the cases or concentrated on the most difficult. The former hypothesis would imply weakness of the classification to discriminate among cases or failure of the raters to recognize certain criteria (insufficient training). In contrast, if the classification performs well, the discrepancies should be concentrated on a small number of difficult cases. A heatmap of diagnostic labels per evaluator indicates that discrepancies clustered around two problematic cases (L13-064 and L13-065, both of which were NRAS-Ink4a tumors) due to poor tumor circumscription (Figure 7b).

3 | DISCUSSION

GEM models of melanoma have been developed over the last two decades to study genotype/phenotype correlations in melanoma development and, to a lesser degree, as a prescreening tool for drugs. Melanocytic lesions in mouse models represent a spectrum that varies from one model to another, similar to human lesions. It is thus important to classify lesions in homogeneous categories in a reproducible and simple manner. Such a classification system should be targeted for use by mouse researchers, even those with minimal training in histopathology, because of the shortage of human and veterinary pathologists involved in animal experimentation. Here, we propose a classification that attempts to address those needs. We developed a classification system for the murine melanocytic lesions (MLP1, MLP2, and MT1 to MT3) in NRAS mouse models, based on nine morphological criteria that only require a routine H&E stain.

In this study, no melanocytic lesion was assigned to the MLP1 category. This is because MLP1 and MLP2 lesions are precursor melanocytic lesions that are not grossly visible. The policy was to harvest
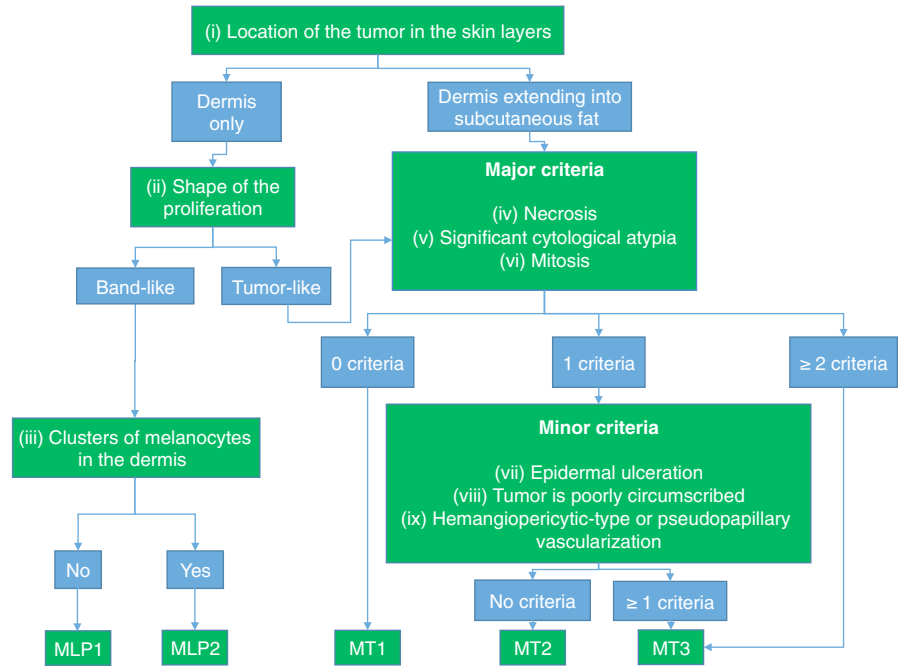
FIGURE 6 Decision tree to classify murine melanocytic lesions for various NRAS melanoma models [Colour figure can be viewed at wileyonlinelibrary.com]

FIGURE 7 Reproducibility of the classification system. (a) Repartition of each diagnostic category according to each rater involved in the study. Repartition between the different categories of the 20 cases included in the panel was similar between raters. The color scheme used corresponds to the different categories of melanocytic lesions. P = Pathologist, R1 = Researcher 1, R2 = Researcher 2. (b) Heatmap of diagnostic categories per rater and case. Rows represent cases, and columns represent raters. Discordant cases and the amplitude of the discrepancy can easily be spotted using this visualization. Color scheme and abbreviations are identical [Colour figure can be viewed at wileyonlinelibrary.com]
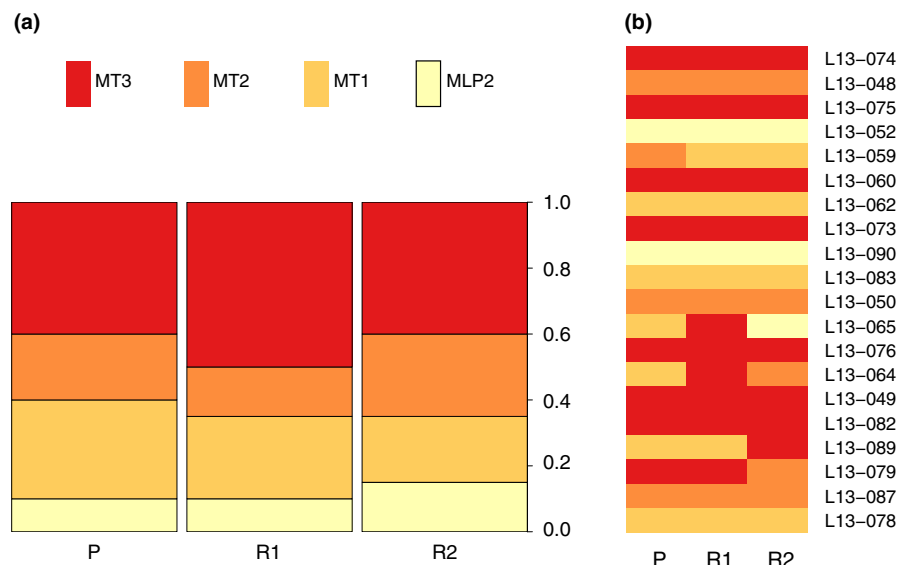
tumors that grew to approximately 1 cm in the largest diameter or when humane endpoints were reached. These lesions were therefore not sampled intentionally. MLP1 and MLP2 lesions almost invariably appeared on the lateral margins of larger melanocytic lesions that fell into the MT1, MT2, or MT3 categories. When association occurred, the MT1, MT2, MT3 categories took precedence for classification purposes.

A few infrequent situations may challenge our classification. Melanocytic lesions may infrequently arise from the subcutaneous tissue or even below the superficial fascia with no visible link to the dermis. An illustration of this aspect is provided (Figure S3). A similar observation has been made by others (Wurm et al., 2012). These authors hypothesized that the tumors arising from the subcutis originate from a population of melanocytes located in the hair bulb. However,

this does not explain the cases that originate from deeper layers. For classification purposes, such cases should be included with tumors located in the dermis that extend into the subcutaneous fat and evaluated for major malignancy criteria (necrosis, mitosis, presence of significant atypia) before proceeding further in the decision tree.

Tumor circumscription was sometimes difficult to evaluate, due to the quantity of melanin-containing macrophages (melanophages) at the periphery of the tumor. This was a cause of discordance between the three observers for two of 20 cases. More generally, the oncogenic activation of NRAS in the C57BL/6 strain results in extreme hyperpigmentation. This hindered the evaluation of mitosis and atypia for some tumors when melanin obscured the nuclear features. This evaluation could thus only be performed on mildly pigmented or unpigmented cells. Bleaching slides with potassium permanganate or dilute

hydrogen peroxide can remove excess pigment and allow for a better view of the morphology, but may alter antibody staining (Ferguson, Soyer, & Walker, 2015; Manicam et al., 2014). Others have advocated the use of an albino inbred FVB background, originally derived from an outbred Swiss colony (Wurm et al., 2012).

The "band-like" pattern that we observed in precursor MLP1 and MLP2 lesions has been described previously in the Tyr::NRAS^{Q61K}; Cdk4$^{R24C/R24C}$ mouse melanoma model (Wurm et al., 2012). The authors did not observe this pattern in Tyr::NRAS^{Q61K}; Tyr::Cre(ER); p53$^{F/F}$; or Tyr::NRAS^{Q61K}; Arf$^{−/−}$ mice. We found this "band-like" pattern in all genotypes examined in our study. This apparent conflict may result primarily from the mouse strains and not melanin content (C57BL/6 versus FVB). Although we did not test all genetic combinations, the proposed classification is certainly applicable to most Tyr::NRAS^{Q61K}-derived models, provided the spectrum of melanocytic lesions is the same. However in our experience, this classification is not applicable to lesions derived from Tyr::CreER$^{T2/°}$; Braf$^{LSL-V600E/+}$ models (Dhomen et al., 2009).

The development of melanocytes during embryogenesis is well conserved between humans and mice, making the latter a suitable model for melanocytic pathology research. However, there are differences between mouse and human melanocyte pathology. In humans, melanocytes are distributed predominantly along the basal layer of the interfollicular epidermis, as well as in the hair follicles. Mouse melanocytes are located primarily in the hair follicles, with very few interfollicular melanocytes in the furry region. As noted by some authors (Perez-Guijarro, Day, Merlino, & Zaidi, 2017), melanocytic lesions in most genetically engineered mouse models mostly develop dermally and share few histological similarities with human melanomas, which have a predominantly epidermal or dermo-epidermal junctional component. However, mouse melanomas are of epidermal origin as melanocytes are located in the hair follicles, an epidermal adnexal structure (Larue, 2012). Instead, murine melanocytic lesions share similarities with the blue nevi spectrum of lesions. Thus, MLP1 and MLP2 lesions share features with common blue nevi and epithelioid blue nevi, whereas MT1, MT2, and MT3 lesions have similarities with the cellular blue nevus/pigmented epithelioid melanocytoma/atypical cellular blue nevus/malignant blue nevus diagnostic spectrum (Mooi, 2001; Zembowicz & Phadke, 2011).

One limitation of our study is that malignant behavior was inferred from morphological criteria alone. Ideally, the malignant potential of a category of melanocytic lesions should be inferred from the presence of metastases. However, animal regulatory ethical requirements often dictate that mice be killed before metastatic disease develops. This scientific endpoint is therefore often not usable because of missing data.

4 | MATERIALS AND METHODS

4.1 | Transgenic mice and tumor collection

The transgenic Tyr::NRAS^{Q61K}/° mouse lines (Tyr::NRAS^{Q61K}), (Tyr::NRAS^{Q61K}/°; Ink4a-Arf$^{+/−}$), (Tyr::NRAS^{Q61K}/°; Tyr::bcat^{sta}/°),

and (Tyr::NRAS^{Q61K}/°; Tyr::Cre/°; Pten$^{F/+}$) have been previously described (Ackermann et al., 2005; Conde-Perez et al., 2015; Delmas, Martinozzi, Bourgeois, Holzenberger, & Larue, 2003; Delmas et al., 2007; Longvert et al., 2011; Serrano et al., 1996). Tyr::NRAS^{Q61K}/°, Ink4a-Arf$^{+/−}$, and Floxed PTEN mice were kindly provided by F. Beermann (EPFL, Lausanne, Switzerland), M. Serrano (CNIO, Madrid, Spain), and H. Wu (UCLA, Los Angeles, CA, USA), respectively. All mice were backcrossed onto a C57BL/6 background for more than 10 generations and maintained in the specific pathogen-free mouse colony at the Curie Institute, in accordance with French and European Union laws (authorization number P2.LL.029.07). Mice were genotyped by PCR using DNA extracted from tails. The mice were evaluated weekly for tumor appearance and progression. Once tumors were 1 cm in diameter, the mice were euthanized and autopsied. Some mice were also sacrificed because of poor health.

4.2 | Histology of mouse tumors

Mouse melanomas were collected, rinsed in cold PBS, and fixed in 4% paraformaldehyde at 4°C O/N. Samples were dehydrated, embedded in paraffin wax, and cut into 5-μm-thick transverse sections. Paraffin-embedded sections were stained with hematoxylin and eosin (H&E) and examined by light microscopy. Histopathological criteria used previously in the classification of Tyr::NRAS^{Q61K} melanocytic lesions included the size of the lesion, location of the tumor in the skin layers, contour/shape of the lesion, cellular density, cell shape, aspect of the nucleus, atypia, mitotic count, pigment abundance, presence and aspect of blood vessels, and presence of necrosis or ulceration (Campagne et al., 2013).

5 | CONCLUSION

We propose a new, simplified, reproducible classification for mouse melanocytic lesions from the Tyr::NRAS^{Q61K} model and various derivatives. Adoption of this classification system should result in a common base for communication between researchers working on melanoma mouse models. It is likely that new melanoma mouse models may require minor changes or a complete overhaul of this classification. We strongly encourage the reader to consult the additional material provided in supplemental data and figures, including an interactive "easy-to-use" classification guide and illustrations for the criteria used.

Fourchardière, Giorgia Egidy, Laurent Le Cam, and Enrico Radaelli for helpful discussions.

CONFLICT OF INTEREST

We declare that we have no conflict of interest.

ORCID

Lionel Larue 🆔 http://orcid.org/0000-0002-2010-6107

REFERENCES

Ackermann, J., Frutschi, M., Kaloulis, K., Mckee, T., Trumpp, A., & Beermann, F. (2005). Metastasizing melanoma formation caused by expression of activated N-RasQ61K on an INK4a-deficient background. *Cancer Research*, *65*, 4005–4011. https://doi.org/10.1158/0008-5472.CAN-04-2970

Barthold, S. W., Borowsky, A. D., Brayton, C., Bronson, R., Cardiff, R. D., Griffey, S. M., … Ward, J. M. (2007). From whence will they come? - A perspective on the acute shortage of pathologists in biomedical research *Journal of Veterinary Diagnostic Investigation*, *19*, 455–456.

Campagne, C., Reyes-Gomez, E., Battistella, M., Bernex, F., Chateau-Joubert, S., Huet, H., … Egidy, G. (2013). Histopathological atlas and proposed classification for melanocytic lesions in Tyr:NRas(Q61K); Cdkn2a(-/-) transgenic mice. *Pigment Cell & Melanoma Research*, *26*, 735–742. https://doi.org/10.1111/pcmr.12115

Cardiff, R. D. (2007). Pathologists needed to cope with mutant mice. *Nature*, *447*, 528. https://doi.org/10.1038/447528c

Cardiff, R. D., Ward, J. M., & Barthold, S. W. (2008). 'One medicine—one pathology': Are veterinary and human pathology prepared? *Laboratory Investigation*, *88*, 18–26. https://doi.org/10.1038/labinvest.3700695

Conde-Perez, A., Gros, G., Longvert, C., Pedersen, M., Petit, V., Aktary, Z., … Larue, L. (2015). A caveolin-dependent and PI3K/AKT-independent role of PTEN in beta-catenin transcriptional activity. *Nature Communications*, *6*, 8093. https://doi.org/10.1038/ncomms9093

Conde-Perez, A., & Larue, L. (2014). Human relevance of NRAS/BRAF mouse melanoma models. *European Journal of Cell Biology*, *93*, 82–86. https://doi.org/10.1016/j.ejcb.2013.10.010

Delmas, V., Beermann, F., Martinozzi, S., Carreira, S., Ackermann, J., Kumasaka, M., … Larue, L. (2007). Beta-catenin induces immortalization of melanocytes by suppressing p16INK4a expression and cooperates with N-Ras in melanoma development. *Genes & Development*, *21*, 2923–2935. https://doi.org/10.1101/gad.450107

Delmas, V., Martinozzi, S., Bourgeois, Y., Holzenberger, M., & Larue, L. (2003). Cre-mediated recombination in the skin melanocyte lineage. *Genesis*, *36*, 73–80. https://doi.org/10.1002/(ISSN)1526-968X

Dhomen, N., Reis-Filho, J. S., Da Rocha Dias, S., Hayward, R., Savage, K., Delmas, V., … Marais, R. (2009). Oncogenic Braf induces melanocyte senescence and melanoma in mice. *Cancer Cell*, *15*, 294–303. https://doi.org/10.1016/j.ccr.2009.02.022

Ferguson, B., Soyer, H. P., & Walker, G. J. (2015). Clinicopathological characterization of mouse models of melanoma. *Methods in Molecular Biology*, *1267*, 251–261. https://doi.org/10.1007/978-1-4939-2297-0

Fleiss, J. L., Levin, B., & Paik, M. C. (2003). *Statistical methods for rates and proportions*. Hoboken, NJ: Wiley. https://doi.org/10.1002/0471445428

Frese, K. K., & Tuveson, D. A. (2007). Maximizing mouse cancer models. *Nature Reviews Cancer*, *7*, 645–658.

Herrington, C. S. (2014). *Muir's Textbook of Pathology*. Boca Raton, FL, USA: CRC Press.

Larue, L. (2012). Origin of mouse melanomas. *The Journal of Investigative Dermatology*, *132*, 2135–2136. https://doi.org/10.1038/jid.2012.221

Larue, L., & Beermann, F. (2007). Cutaneous melanoma in genetically modified animals. *Pigment Cell Research*, *20*, 485–497. https://doi.org/10.1111/j.1600-0749.2007.00411.x

Longvert, C., Gros, G., Beermann, F., Marais, R., Delmas, V., & Larue, L. (2011). Murine cutaneous melanoma models. Importance of the genetic background. *Annales de Pathologie*, *31*, S70–S73. https://doi.org/10.1016/j.annpat.2011.09.002

Manicam, C., Pitz, S., Brochhausen, C., Grus, F. H., Pfeiffer, N., & Gericke, A. (2014). Effective melanin depigmentation of human and murine ocular tissues: An improved method for paraffin and frozen sections. *PLoS One*, *9*, e102512. https://doi.org/10.1371/journal.pone.0102512

Marasini, D., Quatto, P., & Ripamonti, E. (2016). Assessing the inter-rater agreement for ordinal data through weighted indexes. *Statistical Methods in Medical Research*, *25*, 2611–2633. https://doi.org/10.1177/0962280214529560

Mooi, W. J. (2001). The expanding spectrum of cutaneous blue naevi. *Current Diagnostic Pathology*, *7*, 58–68.

Perez-Guijarro, E., Day, C. P., Merlino, G., & Zaidi, M. R. (2017). Genetically engineered mouse models of melanoma. *Cancer*, *123*, 2089–2103. https://doi.org/10.1002/cncr.30684

Quatto, P., & Ripamonti, E. (2014). Raters: A Modification of Fleiss' Kappa in Case of Nominal and Ordinal Variables.

R-Core-Team (2017). *R: A Language and Environment for Statistical Computing*. Vienna, Austria: R Foundation for Statistical Computing.

Serrano, M., Lee, H., Chin, L., Cordon-Cardo, C., Beach, D., & Depinho, R. A. (1996). Role of the INK4a locus in tumor suppression and cell mortality. *Cell*, *85*, 27–37. https://doi.org/10.1016/S0092-8674(00)81079-X

Van Diest, P. J., Baak, J. P., Matze-Cok, P., Wisse-Brekelmans, E. C., Van Galen, C. M., Kurver, P. H., … Kwee, W. S., (1992). Reproducibility of mitosis counting in 2,469 breast cancer specimens: Results from the Multicenter Morphometric Mammary Carcinoma Project. *Human Pathology*, *23*, 603–607. https://doi.org/10.1016/0046-8177(92)90313-R

Weidner, N., Cote, R., Suster, S., & Weiss, L. (2009). *Modern surgical pathology*. Amsterdam, the Netherlands: Elsevier.

Wurm, E. M., Lin, L. L., Ferguson, B., Lambie, D., Prow, T. W., Walker, G. J., & Soyer, H. P. (2012). A blueprint for staging of murine melanocytic lesions based on the Cdk4 (R24C/R24C):Tyr- NRAS (Q)(61K) model. *Experimental Dermatology*, *21*, 676–681. https://doi.org/10.1111/j.1600-0625.2012.01543.x

Zembowicz, A., & Phadke, P. A. (2011). Blue nevi and variants: An update. *Archives of Pathology and Laboratory Medicine*, *135*, 327–336.

SUPPORTING INFORMATION

Additional Supporting Information may be found online in the supporting information tab for this article.

How to cite this article: Sohier P, Legrand L, Aktary Z, et al. A histopathological classification system of Tyr::NRAS^{Q61K} murine melanocytic lesions: A reproducible simplified classification. *Pigment Cell Melanoma Res.* 2018;31:423–431. https://doi.org/10.1111/pcmr.12677